Assessing extraction trail trafficability using harvester CAN-bus data

Jari Ala-Ilomäki , Aura Salmivaara , Samuli Launiainen , Harri Lindeman , Sampo Kulju , Leena Finér , Jukka Heikkonen & Jori Uusitalo

Published online: 02 May 2020.

Submit your article to this journal ⃗

Article views: 216

View related articles ⃗

View Crossmark data ⃗

Assessing extraction trail trafficability using harvester CAN-bus data

Jari Ala-Ilomäki [a], Aura Salmivaara[b], Samuli Launiainen[b], Harri Lindeman[a], Sampo Kulju[a], Leena Finér [b], Jukka Heikkonen[c] and Jori Uusitalo[a]

aNatural Resources Institute Finland, Department of Production Systems, Helsinki, Finland; bNatural Resources Institute Finland, Department of Natural Resources, Helsinki, Finland; cUniversity of Turku, Department of Future Technologies, Turku, Finland

ABSTRACT

Modern forest machines with a Controlled Area Network (CAN)-bus managed diesel engine and hydrostatic transmission can continuously measure power expended in traveling. At a constant speed on level ground, the power is expended in overcoming motion resistance, which is directly related to wheel sinkage and hence to site trafficability. In cut-to-length timber harvesting, the harvester precedes the forwarder on the site, making it feasible to utilize the harvester to collect data on site trafficability to produce a trafficability map for the forwarder. CAN-bus trafficability mapping was tested with an 8-wheeled Ponsse Scorpion King harvester and an 8-wheeled Ponsse Elk forwarder instrumented for collecting transmission power expenditure, in addition to appropriate available CAN-bus information. Trafficability was also mapped based solely on momentary engine power in order to eliminate the need for additional pressure transducers. The CAN-bus data showed good results for mapping site trafficability when compared to soil penetration resistance and harvesting machinery wheel rut depth measurements. Assessing harvester rolling resistance using CAN-bus data offers an interesting possibility to map harvesting site trafficability also in Big Data scale. Since modern harvesters are practically ready for indirect power recording, the additional cost of fully automated and comprehensive trafficability mapping as part of operative forestry is negligible.

Introduction

In Finland, and the Boreal region as a whole, the high season for timber harvesting has traditionally been winter when the increased bearing capacity of frozen ground can be utilized. The seasonal variation in timber harvesting is, however, estimated to cause additional annual costs of 100M€ to the Finnish forest sector (Pennanen and Mäkelä 2003). Thus, to secure a continuous flow of timber, forestry operations need to be more evenly distributed over the year. This emphasizes the need for forest terrain trafficability prediction, not only in avoiding soil damage by heavy forest machines but also in improving the economy of timber harvesting. Avoiding soil damage is important in maintaining the productivity of forest soil and for the acceptability of timber harvesting by private forest owners, who own two thirds of the growing stock in Finland (Finnish forest statistics 2018). A major fraction of private owners are less dependent on the income from the forest and may prioritize recreational and nature conservational values. The public acceptability of timber harvesting is also becoming increasingly important. Besides avoiding wheel ruts, increasing attention has lately been paid to reducing soil compaction by forest machines (Toivio et al. 2017).

Timber harvesting in the Nordic countries is carried out almost entirely by specific cut-to-length harvesting machinery. While being highly effective, the machinery has also become remarkably heavy, with a typical harvester weighing 22 000 kg and an unloaded forwarder 18 000 kg. Operating with heavy machinery can cause harmful rutting, especially on peat soils and in thinning stands. The problem is serious since a quarter of the growing stock is on peatland, and roughly 40% of annual timber removal is from thinning cuttings (Finnish Statistical Yearbook of Forestry 2014).

Presently, a harvesting operation foreman and a machine operator estimate the trafficability of a harvesting site on the basis of their field experience. The estimation is, however, often challenging and inaccurate because trafficability conditions vary considerably across and between sites and as a result of varying weather conditions. Thus, more accurate predictions of trafficability would currently require *in-situ* visits preceding the planned operation date, which is costly and hence avoided as much as possible.

Operational methods for predicting soil trafficability based on weather information and site characteristics do not yet exist in Nordic countries. Initial operational decision support tools are under development (Bergqvist et al. 2017a, 2017b). The lack of prediction models is, to a large extent, due to a lack of data on soil trafficability. Point specific soil strength measurements are too expensive to be gathered to sufficiently cover the variability in site conditions due to soil texture, topography and weather-induced changes in soil moisture and frost depth. Therefore, novel low-cost methods for collecting extensive, spatially and temporally explicit data on soil trafficability are needed. Suvinen and Saarilahti (2006) proved the applicability of forwarder hydraulic driveline CAN-bus data for measuring mobility parameters. Using the harvester CAN-bus measured proxies of trafficability collected during

CONTACT Jari Ala-Ilomäki jari.ala-ilomaki@luke.fi Natural Resources Institute Finland, Box 2, Helsinki FI-00791, Finland

operational harvesting to create a trafficability map of the extraction road network for the heavier forwarder would be a feasible solution. Harvester operators will in the future have the information supplied by depth-to-water maps and dynamic soil trafficability maps based on weather information. In cut-to-length thinning however, the harvester has to cover the site at a 20 meter extraction road spacing, which will result in machine travel over wet areas. The harvester CAN-bus measured trafficability proxies would help the forwarder operator to avoid heavy loading on soft areas. Equipping the harvesting machinery fleet with an automatic trafficability measuring system would also enable the rapid collection of data in varying site, soil and weather conditions – a prerequisite for improving the trafficability models.

Our aim was to study whether the extraction trail trafficability can be assessed by using the CAN-bus data continuously collected by forest machinery. To achieve this goal, we collected CAN-bus data and measured rut depth in a field trial mimicking a normal thinning operation. The harvester rolling resistance and its spatial variability was estimated on the basis of CAN-bus data and its use as a trafficability proxy evaluated against rutting caused by successive harvester and forwarder passes. The results can be used to develop a low-cost solution ready to be piloted in forest operations and applicable to forest machine production.

CAN-bus measurement system

Measurement principle

On level ground and at a constant speed (i.e. acceleration equal to zero), engine torque led through a hydrostatic-mechanical transmission to the driving gear is expended in overcoming internal friction and motion resistance (Suvinen and Saarilahti 2006; Ala-Ilomäki et al. 2012). In real off-road conditions, the power expended is further dependent on a number of factors, such as slope resistance and acceleration

(Figure 1). The efficiency of the hydraulic transmission and mechanical transmission following it in the transmission path to the running gear must also be taken into account.

The mapping of extraction trail trafficability with the harvester preceding the forwarder on a logging site is thus possible by collecting the necessary data from the harvester CAN-bus channel (Ala-Ilomäki et al. 2012). The measured expended power, corrected by factors such as slope force is divided by the forward travel speed of the vehicle to obtain the rolling resistance force which is dependent on wheel sinkage. Determining the forward travel speed can be accomplished by a satellite navigation device. This is not the most accurate method in forestry conditions, especially in Nordic conditions with less favorable GPS satellite positions, yet the data are readily available from a modern forest machine, and the introduction of Glonass positioning has improved positioning accuracy. The increase in rolling resistance with higher running gear sinkage forms the basis on CAN-bus based trafficability mapping. The end result is rolling resistance coefficient, a proxy of terrain trafficability as determined by soil bearing capacity.

Direct measurement of transmission power

In principle, the most accurate method for determining the power expended in machine travel on the basis of CAN-bus data is to measure the differential hydraulic pressure and flow rate of the transmission. The product of these, multiplied by the coefficient of hydraulic efficiency yields power (Equation (1)). Hydraulic efficiency is affected by the wear of hydraulic transmission components.

$$P_h = p_{hdiff} \times q \times \eta_h \tag{1}$$

P_h = Hydraulic power (kW), p_{hdiff} = Differential hydraulic pressure (kPa), q = Flow rate (m³s⁻¹), η_h = Coefficient of hydraulic efficiency.
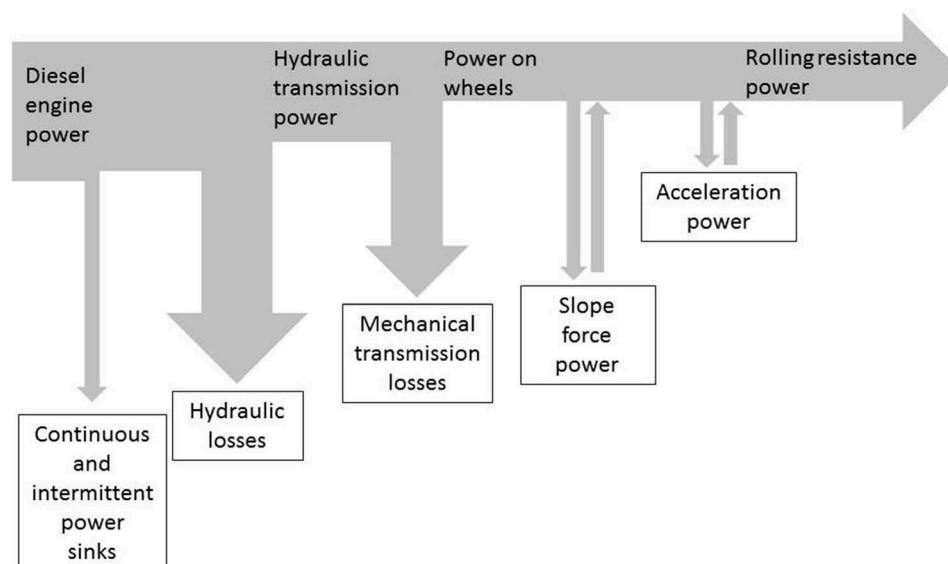

Figure 1. Schematic of the division of harvester diesel engine power in overcoming rolling resistance. Slope and acceleration resistance may either increase or decrease the calculated power expended in overcoming the rolling resistance.

If pressure data are not readily available, transducers have to be mounted to measure the input and output pressure of the transmission hydraulic pump. The flow rate can be assessed by recording the transmission control data for flow rate. In the test drives, the transmission hydraulic power was determined based on the differential pressure over the hydraulic pump, motor volume per one rotation set by the transmission control unit, the hydraulic unit rotational speed and the hydraulic efficiency. The formula (Equation (2)) for calculating the direct method hydraulic power of this particular transmission setup was supplied by Ponsse Plc. The need for additional transducers makes direct measurement less desirable for production applications.

$$P_{hdir} = ((n_m \times 60 \times (I_m \times a_1 + b_1)/\eta_{m\ vol} \times 1000) \times p_{hdiff})/1000 \tag{2}$$

$a_1 = (V_{m\ max} - V_{m\ min})/(I_{m\ min} - I_{m\ max}), b_1 = a_1 \times I_{m\ min} + V_{mmax}$, P_{hdir} = Directly measured hydraulic power (kW), n_m = Hydraulic motor rotational speed (s^{-1}), I_m = Hydraulic motor control current (mA), $\eta_{m\ vol}$ = Coefficient of motor volumetric efficiency, $V_{m\ max}$ = Hydraulic motor maximum displacement per revolution (cm^3), $V_{m\ min}$ = Hydraulic motor minimum displacement per revolution (cm^3), $I_{m\ min}$ = Hydraulic motor minimum control current (mA), $I_{m\ max}$ = Hydraulic motor maximum control current (mA).

Indirect measurement of transmission power

An indirect way of assessing power expended in machine travel is by using momentary diesel engine power determined on the basis of torque and engine speed read from CAN-bus (Equation (3)). Since engine power is not entirely converted into hydraulic power, the efficiency of the engine-hydraulic transmission system η_{eh} has to be determined (Equation (4)). In latter analysis, η_{eh} is represented by the slope and the constant term of the linear regression equation. In case the hydraulic components of the transmission are not factory-equipped for appropriate transducers, this would be a cost-effective way to build the measuring system in a production application as no additional instrumentation is needed. The engine power to hydraulic power efficiency is affected by the wear of hydraulic transmission components. Additionally, engine power is consumed by continuous and intermittent auxiliary power sinks such as an alternator, cooling fans and articulated steering. The duration of the intermittent power sinks can be traced from CAN-bus data.

$$P_{eng} = T \times n_{eng} \times 2 \times \pi \tag{3}$$

$$P_{hind} = P_{eng} \times \eta_{eh} = a_2 \times P_{eng} + b_2 + e \tag{4}$$

P_{eng} = Engine power (kW), T = Engine torque (kNm), n_{eng} = Engine rotational speed (s^{-1}), P_{hind} = Hydraulic power measured indirectly (kW), η_{eh} = Coefficient of engine power to hydraulic power efficiency, a_2 = Slope, b_2 = Constant term (kW), e = Error term.

Rolling resistance calculus

The determination of diesel engine power (Figure 1) was based on engine control unit calculated torque and engine speed read from the CAN-bus. The CAN-bus data were directly obtained from the Ponsse Opti control system, whereas the hydraulic pressure transducer data were recorded with an additional datalogger supplied by Creanex Ltd. The engine output to transmission hydraulic power conversion efficiency was determined by collecting both direct hydraulic power and engine output measurement data simultaneously in reference test drives on a collector trail. A linear model (Equation (4)) was fitted to the data and used to convert engine power into indirectly measured transmission power in actual test drives.

In the tested harvester, the hydraulic transmission is followed by a conventional mechanical transmission consisting of a drop box, final drives, gears inside the bogies, and finally a wheel hub reduction. The total number of gear meshes with an assumed coefficient of efficiency of 0.97 was 10, resulting in an overall 0.74 coefficient of mechanical efficiency (Equation (5)). The transmission hydraulic power, determined directly (Equation (2)) or indirectly (Equation (4)), was multiplied by the efficiency of the mechanical transmission to obtain power acting on wheels (Equation (6)).

$$\eta_{mech} = \eta_m^n \tag{5}$$

$$P_w = P_h \times \eta_{mech} \tag{6}$$

η_{mech} = Coefficient of efficiency of mechanical transmission, η_m = Coefficient of efficiency of single gear mesh, n = Number of gear meshes, P_w = Power acting on wheels (kW), P_h = Hydraulic power (kW).

During normal work in easy terrain conditions, such as those which prevailed on the test sites, both the harvester and forwarder typically travel at near-constant speed. On the test sites, the harvester stopped for cutting and then moved to the next work station, whereas the forwarder was loaded before the test drives and was therefore able to travel through the test sites nonstop. The acceleration of the machines was not measured separately and the frequency of the collected GPS data was too low for this purpose. Acceleration was thus dealt with by selecting a subset of data from the speed range 0.5 to 1.0 ms^{-1}, where the harvester had reached the near-constant speed. Given the considerable mass of the harvester, accelerations and decelerations were minor and assumed here to cancel out each other. Measurements by Suvinen and Saarilahti (2006) support this assumption.

Since the test sites were laid out as straight as possible, the effect of turning resistance and the power expended by articulated steering were omitted. Also the effect of obstacle resistance was omitted. The cooling of the hydraulic system of a modern full-size harvester is a big power sink and it was therefore assured that the cooling fan was not switched on during the tests drives.

The determination of vehicle speed needed for converting expended power into motive force (Equation (7)) was based on the machine GPS data. Any possible mismatch in the

timestamps of CAN-bus and GPS data, and that acquired by the additional datalogger, was accounted for by determining a constant lagtime that maximized the correlation between the two data streams.

$$F_m = P_w/v \qquad (7)$$

F_m = Motive force (kN), v = Vehicle speed (ms^{-1}).

Taking slope force into account, the slope angle in the direction of travel was determined on the basis of the 2 m by 2 m digital elevation model (DEM, National Land Survey of Finland 2017) with a vertical accuracy of 0.3 m and the GPS path recorded during the test drives. To obtain rolling resistance, slope force was added to motive force when driving downhill and subtracted from motive force when driving uphill (Equation (8)). Finally, the rolling resistance coefficient was calculated by dividing rolling resistance by the normal component of vehicle weight (Equation (9)).

$$F_r = F_m \pm F_s \qquad (8)$$

$$\mu_r = F_r/N \qquad (9)$$

F_r = Rolling resistance (kN), F_s = Slope force (kN), N = Normal component of vehicle weight (kN), μ_r = Rolling resistance coefficient.

All data preparations and analyzes were performed with R software (R Core Team 2018).

Materials and methods

To test the proposed approach to estimate forest harvester rolling resistance and its spatial variability, a field study was conducted in mid-May 2016 in Vihti, Southern Finland (60° 24′N, 24°23′E in WGS84). To evaluate the applicability of the CAN-bus derived trafficability estimate method, directly measured hydraulic transmission power P_{hdir} was first determined as a function of engine power P_{eng} on a collector trail with a good bearing capacity to obtain the factors for indirect transmission power measurement Equation (4). The CAN measurement principle was then tested on an even forest road with a gravel surface to obtain baseline values for rolling resistance.

For trials in an operational forest environment, a test track of 1.1 km, also used in Salmivaara et al. (2018), was designed. The track (Figure 2) passed through various soil types, including a till-covered bedrock, clay covered by a thin organic layer, and till covered by a dense organic layer of between 10 to 40 cm. The terrain profile varied from flat to slightly undulating, and soil moisture conditions from wet to dry. Along the test track, nine 20 m long straight test sites (later referred to as sites 1 to 9) were selected. The measured average slope angles of the test sites in the direction on harvester travel are given in Table 1.

Both the indirect and the direct measuring principles were tested on the forest road and test sites 1 to 4. On test sites 5 to 9 only the indirect measurement principle was used.

The test track was first driven by an 8-wheeled Ponsse Scorpion King harvester with a mass of 22 500 kg. The rear wheels of each bogie were equipped with OFA Matti chains. During its pass, the harvester opened up the test track by cutting the timber in a manner similar to a normal thinning operation, which necessitated frequent stops along the way. Thereafter, a loaded 8-wheeled Ponsse Elk forwarder with a total mass of 30 000 kg passed the route 2 to 4 times with a near constant speed and alternating driving directions. The rear wheels of the front bogie were equipped with OFA Matti chains while the rear bogie was equipped with 910 mm wide Olofsfors Eco Tracks. Both machines were equipped with Nokian Forest King F2 710/45-26.5 tires.

Penetration resistance was measured on each test site after the harvester pass between wheel ruts at one meter intervals with an Eijkelkamp Penetrolologger 0615SA penetrometer and a 60 ° 1 cm^2 cone (Eijkelkamp Soil&Water 2018), totaling 20 measurements per site. The maximum penetration depth of the device was 80 cm. Depending on the stoniness of the site, two to four 60 mm diameter mineral soil samples per test site were taken with a corer for particle size analysis. These samples were taken from the 0 to 200 mm mineral soil layer, except on shallow soils on bedrock where they were only taken from the 0 to 100 mm mineral soil layer. The depth of both wheel ruts were manually measured after each vehicle pass at one meter intervals with a 1 cm accuracy using a horizontal hurdle and a measuring rod. The rut measurement location was marked on the ground with spray paint to enable measurements from the same location on consecutive vehicle passes (Salmivaara et al. 2018). Test site 2 was covered with logging residue to determine the effect of a brush mat commonly used in practical harvesting operations to protect soil from excessive disturbance, whereas other test sites were clear of logging residue. Accurate GPS coordinates of the start and end points of the test sites were recorded.

Results

Soil and terrain conditions

Test sites 1, 2 and 5 were located on bedrock hilltops with a shallow soil deposit. In addition, the surface of site 5 was fairly rough due to large cobbles and boulders. Sites 3 and 8 were located in wet terrain recessions and site 6 in a wet valley. Site 9 was adjacent to site 8, on a slightly higher elevation. Sites 4 and 7 were former agricultural fields on gentle slopes. On the basis of a particle size analysis, the mineral soil types on the study sites were classified according to Karlsson and Hansbo (1981) into even-graded soils and tills (Figure 3). Test site 6 was fine sand and site 9 medium sand; sites 1, 2, and 5 were silty sand till; sites 3 and 8 sandy silty clay till, and sites 4 and 7 silty clay till.

The average penetration resistance down to average penetration depth on the test sites is presented in Figure 4. The sites can be divided into two groups: on the wet sites (3, 6, 8 and 9), the penetration resistance was lower on the surface layer down to 35 cm than that of the other, drier sites. Sites 1, 2 and 5 on bedrock had a shallow penetration depth with penetration resistance shooting up upon meeting the bedrock surface. The penetration resistance measured on site 2 did not describe its high bearing capacity, as the shallow layer of soil
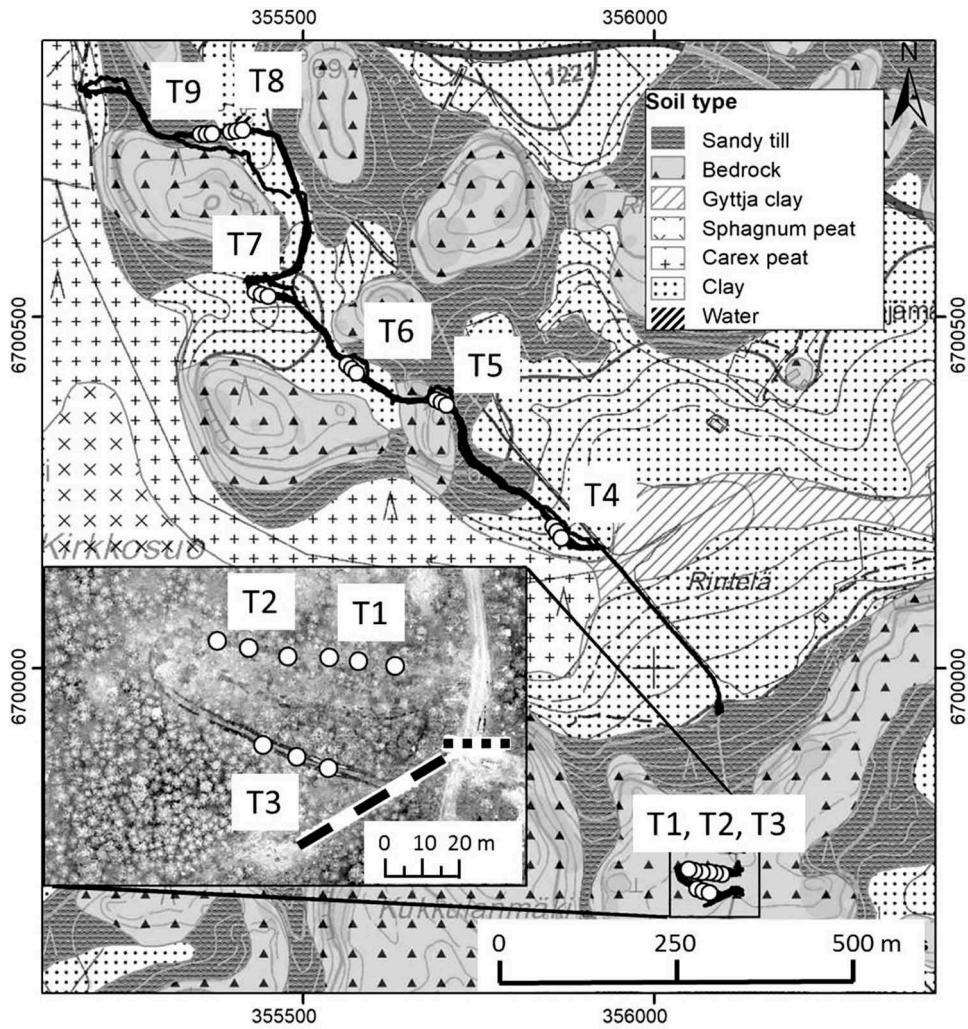
Figure 2. Field test route (black line) and the nine 20-m-long test sites (white dots) located on various soil types. Test sites T1–T3, collector trail test site (dashed line) and gravel road test site (dotted line) are enlarged into an aerial photo. Source for soil map: GSF 1:20,000 (2015), for base map: NLS Topographic database (2017).

Table 1. Average slope angles on the test sites in the direction of harvester travel.

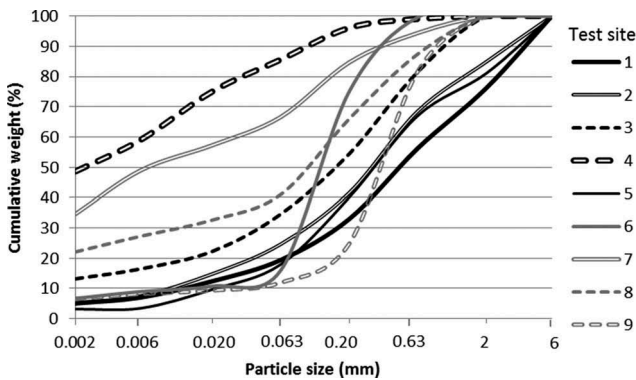|		Test site									
	Transmission efficiency test	Gravel road	1	2	3	4	5	6	7	8	9
Average slope, °	0.0	0.0	3.1	0.0	−0.2	4.0	0.0	0.1	−1.2	0.1	−3.0

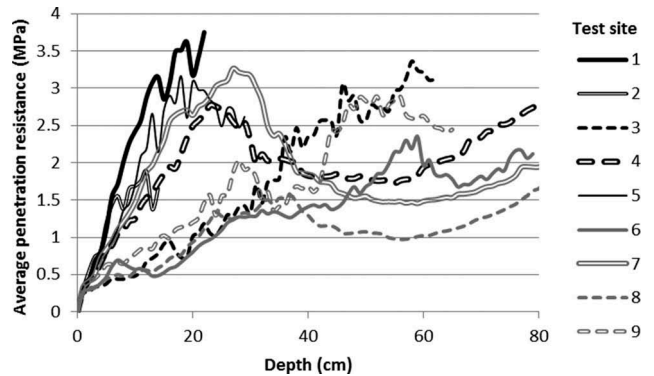**Figure 3.** Particle size (logarithmic scale) distribution of the test site soil samples.

Figure 4. Average penetration resistance down to the average penetration depth on the test sites.

on top of the bedrock seemed to be fairly loose, and the bearing capacity of the bedrock supporting vehicular traffic did not show in the measurement results. Clayey sites 4 and 7 had a dry core layer with a high resistance to penetration.

The average penetration resistance of the top 20 cm layer of mineral soil and the average maximum penetration depth per site are presented in Figure 5. Sites 1, 2 and 5 on bedrock were easily distinguished by a shallow penetration depth. Site 3 was located on the same hilltop as sites 1 and 2. Hence its soil layer was shallower than those of the other sites with a low penetration resistance (6 and 8).

CAN-bus measured rolling resistance and trafficability

Linear regression analysis of directly measured hydraulic transmission power P_{hdir} and engine power P_{eng} on the collector trail resulted in Equation (4) with slope $a_2 = 0.655$ and constant term $b_2 = -30.957$ kW (N = 6445, adjusted $R^2 = 0.676$, residual std error = 4.5 kW).

Direct (Equation (2)) and indirect (Equation (4)) power measurement were then compared in the harvester rolling resistance coefficient calculus on occasions where both methods were applied (Figure 6). The results of the indirect power measurement were highly correlated with the direct measurement results (r = 0.97).

The harvester rolling resistance coefficients and rut depths for the harvester and the forwarder, as averages per test site and
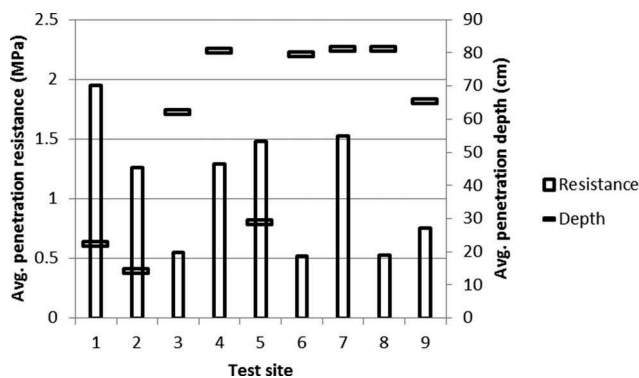

Figure 5. Average penetration resistance of the 20 cm top layer of mineral soil and average maximum penetration depth on the test sites.
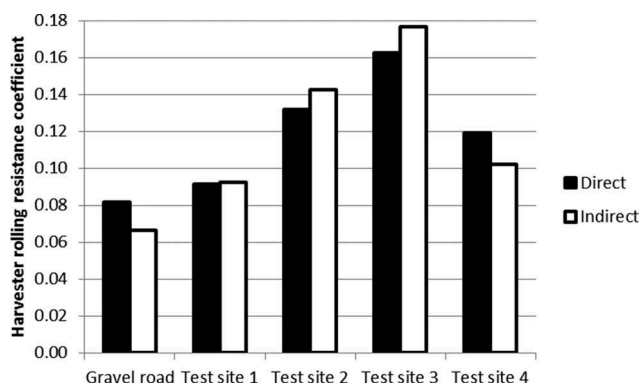

Figure 6. Average direct vs. indirect rolling resistance coefficients calculated for the gravel road and test sites 1 to 4.

vehicle pass, are presented in Figure 6. The highest harvester rolling resistance values were measured on test sites 3, 6 and 8, on which the highest harvester and forwarder rut depths were also observed (Figure 7). The effect of the low soil strength on sites 3, 6 and 8 (Figure 5) were seen in the rut depths and the number of forwarder passes evaluated. The average penetration resistance in the top 20 cm soil layer among sites 3, 6 and 8 did not differ significantly. The average penetration depth on site 3 was the shallowest, and the resistance deeper in the soil was the highest. The soil strength of site 9 would have permitted further passes but the sitehad to be entered through site 8 which was no longer trafficable. The rolling resistance coefficient on site 9, when compared to the moderate rut formation, thus well describes its trafficability despite the low number of passes.

On sites with a shallow soil layer on the top of the bedrock and a good bearing capacity, low values of harvester rolling resistance were expected. This was especially the case on site 1 where the rolling resistance coefficient was the lowest and the rut depth among the lowest of all test sites. The penetration resistance measurements indicated the soil on top of the bedrock was weaker on site 2, but the depth to the bedrock was shallower. Site 2 had a brush mat, which could be a reason for the higher rolling resistance compared to site 1. Also site 5 had a high soil strength and a low rut depth, but the obstacle resistance induced by the surface roughness may have increased the measured rolling resistance coefficient.

Rolling resistance coefficients on the clayey sites 4 and 7 were somewhat inconclusive. On site 7, rolling resistance was especially higher than could be expected based on the measured high penetration resistance and low rut depth (Figures 5 and 7). Judged on the soil strength and rut depth values, the rolling resistance coefficient on site 7 should have been lower than on site 4. The indirect measurement resulted in an underestimation of rolling resistance on site 4 (Figure 6), and thus the real difference between 4 and 7 may not be as large as it appears to be in Figure 7. The rolling resistance on site 7 was high and was similar to site 9, which had clearly weaker soil resulting in deeper ruts.

Discussion

According to the study results, the extraction trail trafficability can be assessed by using the CAN-bus data continuously collected by forest machinery. This supports the findings of Suvinen and Saarilahti (2006). The harvester rolling resistance and its spatial variability could be estimated on the basis of CAN-bus data without the need for any additional transducers. The sites with the poorest bearing capacity were detected best. The sites with good trafficability stood out less clearly. A brush mat was found to decrease rut formation, which is in accordance with previous findings (Uusitalo and Ala-Ilomäki 2013; Poltorak et al. 2018). In good soil bearing conditions, Sirén et al. (2013) found only a small effect of a brush mat on rut depth, and in the present study a brush mat was found to increase the rolling resistance on soil with a good bearing capacity. The indirect measurement principle would be suitable especially for practical big data applications where the amount of data collected is considerable. Since soil strength has an effect also on tractive force, the variable most suited for trafficability mapping would be net traction coefficient. Its determination could be possible by
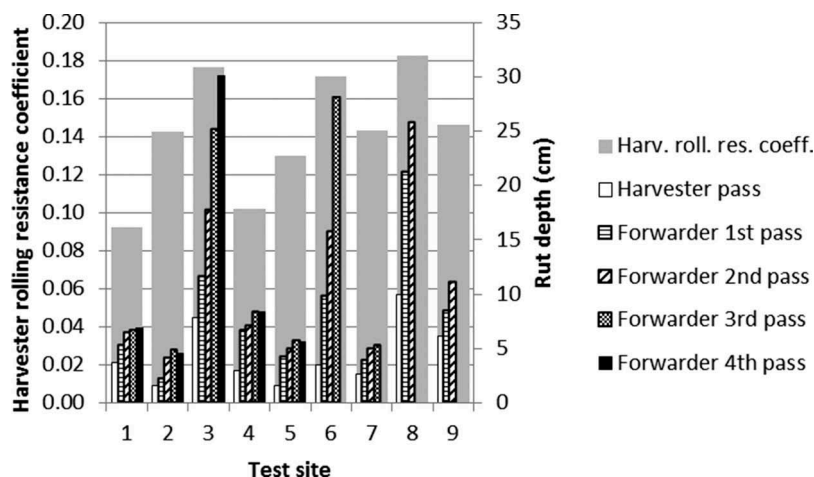
Figure 7. Indirectly measured rolling resistance coefficients for the harvester per test site (wide gray column) and average rut depths for the harvester and the forwarder per test site and vehicle pass (narrow columns starting with the harvester pass on the left).

monitoring harvester wheel slip in frequent stop-and-go cycles characteristic to timber cutting with a harvester.

In conclusion, assessing forest harvester rolling resistance by CAN-bus data offers an interesting possibility to map harvesting site trafficability by actually measuring mobility variables during machine work. Not only is this a leap forward compared to the prevailing human estimation of trafficability, but it is also very cost-effective and will allow collecting spatially and temporally extensive trafficability data supplementing the trail network planning and dynamic site trafficability prediction tools under development. There are no obstacles in piloting the proposed solution for collecting rolling resistance data as part of standard forest operations. Since modern harvesters are practically ready for indirect power recording, the additional cost of trafficability mapping is negligible. If the system was to be employed in all new harvesters, the database on trafficability conditions would buildup rapidly. This can open new intriguing possibilities to develop and validate dynamic trafficability models to support environmentally and economically sound forestry in Nordic countries and elsewhere in the Boreal region (Suvinen 2006; Vega-Nieva et al. 2009; Campbell et al. 2013; Jones and Arp 2017). Trafficability forecast maps would not only serve as input for the optimization of timber transport to the roadside, but also support decision-making on forwarding scheduling, optimal machine size and equipment.

Acknowledgements

Disclosure statement

No potential conflict of interests was reported by the authors.

Funding

Geolocation information

60°24′N, 24°23′E in WGS84

ORCID

Jari Ala-Ilomäki http://orcid.org/0000-0002-6671-7624
Leena Finér http://orcid.org/0000-0001-7623-9374

References

Ala-Ilomäki J, Lamminen S, Sirén M, Väätäinen K, Asikainen A. 2012. Using harvester CAN-bus data for mobility mapping. Mezzinatne. 25 (58):85–87.

Bergqvist I, Willén E, Peuhkurinen J, Väätäinen K, Lindeman H, Laurén A, Poikela A. 2017a. EFFORTE, Big Data bases and applications, D 3.3 Forest trafficability maps – data sources and methods. [accessed 2018 Jun 11]. https://www.luke.fi/efforte/wp-content /uploads/sites/14/2017/09/EFFORTE-D3.3-Forest-trafficability-maps-data-sources-and-methods.pdf.

Bergqvist I, Willén E, Väätäinen K, Lindeman H, Uusitalo J, Laurén A, Peuhkurinen J. 2017b. EFFORTE, Big Data bases and applications, D3.4 Planning for precision forestry by means of trafficability maps. [accessed 2018 Jun 11]. https://www.luke.fi/efforte/wp-content /uploads/sites/14/2017/09/EFFORTE-D3.4-Planning-for-precision-forestry-by-means-of-trafficability-maps.pdf.

Campbell D, White B, Arp P. 2013. Modeling and mapping soil resistance to penetration and rutting using LiDAR-derived digital elevation data. J Soil Water Conserv. 68:460–473. doi:10.2489/jswc.68.6.460.

Eijkelkamp Soil&Water. 2018. Penetrologger with GPS, standard set. [accessed 2018 May 30]. https://en.eijkelkamp.com/products/field-measurement-equipment/penetrologger-set-a.html.

Finnish forest statistics. 2018. Natural Resources Institute Finland. [accessed 2019 Feb 19]:[188 p.]. https://stat.luke.fi/sites/default/files/ suomen_metsatilastot_2018_verkko.pdf.

Finnish Statistical Yearbook of Forestry. 2014. Finnish Forest Research Institute. [accessed 2018 Jun 11]:[426 p.]. https://stat.luke.fi/sites/ default/files/vsk14_koko_julkaisu.pdf.

Jones M, Arp PA. 2017. Relating cone penetration and rutting resistance to variations in forest soil properties and daily moisture fluctuations. Open J Soil Sci. 7:149–171. doi:10.4236/ojss.2017.77012.

Karlsson R, Hansbo S. 1981. Soil classification and identification. Performance and interpretation of laboratory investigations, part 2. Stockholm (Sweden): Swedish Council for Building Research; p. 49. ISBN 91-540-3517-1.

National Land Survey of Finland. 2017. Elevation model 2008–2017, 2 m x 2 m, 2015-10-08, CSC, National Land Survey of Finland (data distributor). [accessed 2016 Jun 1]. http://www.maanmittauslaitos.fi/en/e-services/open-data-file-download-service.

Pennanen O, Mäkelä O 2003. Raakapuukuljetusten kelirikkohaittojen vähentäminen. Metsäteho Ltd. Tech Rep 153.

Poltorak BJ, Labelle ER, Jaeger D. 2018. Soil displacement during ground-based mechanized forest operations using mixed-wood brush mats. Soil Tillage Res. 179:96–104. doi:10.1016/j.still.2018.02.005.

R Core Team. 2018. R: a language and environment for statistical computing. Vienna (Austria):R Foundation for Statistical Computing.

Salmivaara A, Miettinen M, Finér L, Launiainen S, Korpunen H, Tuominen S, Heikkonen J, Nevalainen P, Sirén M, Ala-Ilomäki J, et al. 2018. Wheel rut measurements by forest machine-mounted LiDAR sensors – accuracy and potential for operational applications? Int J For Eng. 29:41–52.

Sirén M, Ala-Ilomäki J, Mäkinen H, Lamminen S, Mikkola T. 2013. Harvesting damage caused by thinning of Norway spruce in unfrozen soil. Int J For Eng. 24:60–75.

Suvinen A. 2006. A GIS-based simulation model for terrain tractability. J Terramech. 43:427–449. doi:10.1016/j.terra.2005.05.002.

Suvinen A, Saarilahti M. 2006. Measuring the mobility parameters of forwarders using GPS and CAN bus techniques. J Terramech. 43:237–252. doi:10.1016/j.terra.2005.12.005.

Toivio J, Helmisaari H-S, Palviainen M, Lindeman H, Ala-Ilomäki J, Sirén M, Uustalo J. 2017. Impacts of timber forwarding on physical properties of forest soils in southern Finland. Forest Ecol Manag. 406:22–30. doi:10.1016/j.foreco.2017.09.022.

Uusitalo J, Ala-Ilomäki J. 2013. The significance of above-ground biomass, moisture content and mechanical properties of peat layer on the bearing capacity of ditched pine bogs. Silva Fenn. 47(3):18. article id 993. doi:10.14214/sf.993.

Vega-Nieva DJ, Murphy PN, Castonguay M, Ogilvie J, Arp PA. 2009. A modular terrain model for daily variations in machine-specific forest soil trafficability. Can J Soil Sci. 89:93–109. doi:10.4141/CJSS06033.